Corrosion Behavior of Annealed Steels with Different Carbon Contents (0.002, 0.17, 0.43 and 0.7% C) in Freely Aerated 3.5% NaCl Solution

Prvan Kumar Katiyar, S. Misra, and K. Mondal

Four annealed carbon steels with different carbon contents (0.002, 0.17, 0.43, and 0.7% C), consisting of ferrite, ferrite-pearlite and fully pearlite microstructures, were selected to understand the corrosion behavior of carbon steel as a function of carbon content in freely aerated 3.5% NaCl solution. Dynamic polarization, electrochemical impedance and linear polarization methods were used. The corrosion rate obtained from the different carbon steels was found to increase greatly from ultra-low carbon steel (0.002%) to low carbon steel (0.17%) due to the presence of pearlite in the low carbon steel. However, the increase in corrosion rate was marginal with the increase in carbon content from low carbon (0.17%) to medium (0.43% C) and high carbon steels (0.7% C). The mirostrucural evolution of the steels before and after polarization test without etching as observed by scanning electron microscopy could show that the corrosion behavior of the steels with the presence of pearlite was due to the combined effect from % pearlite, interlamellar spacing and cementite/ferrite area ratio in pearlite. Pearlite morphology also led to the differential corrosion within the pearlite colony in all the steels except the steel with 0.002% C. Catalytic activity of cementite on enhancing oxygen reduction reaction attributes to the higher corrosion rates in case of the steels with the presence of pearlite.

1. Introduction

The mechanical and electrochemical properties of steel are directly interconnected to the chemistry, processing route and resulting microstructure of the selected steel. The plain carbon steel has vast ranges of applications too. Interstitial-free (IF) or ultra-low carbon steels are widely used in automobile applications due to their excellent formability (Ref 1, 2). The ferrite-pearlite steels with 0.17 and 0.43% C steels are mostly used as a beam in bridges, buildings, ships and reinforcing bars (Ref 3). Steel with high carbon ($\sim$ 0.77%) and fully pearlite microstructure is widely used in rail making (Ref 4).

Corrosion behavior of the plain carbon steel is also strongly influenced by the composition, especially content of C, Si and Mn (Ref 5). On the other hand, various researchers have tried to develop corrosion-resistant steels at minimum alloying addition. In this regard, they have altered the chemistry of the steel by changing C, Si and Mn contents,

which not only offer the excellent strength to the materials, but they also influence the corrosion resistance (Ref 4, 6). The effect produced by Si and Mn is relatively complex, while the increase in C leads to the formation of cementite (Fe_3C), which results in the development of galvanic couple between the ferrite (anode) and cementite (cathode) phases resulting in higher corrosion rates (Ref 7). Hence, the modification in the microstructures of steel is an effective way to improve the corrosion resistance of the plain carbon steel. Further alloying with Cu, Ni and Cr could effectively increase the corrosion resistance of low alloy plain carbon steel (Ref 8). Moon et al. (Ref 9) have also investigated the passivation behavior of ferrite-pearlite railway axle steels based on composition and microstructure and found better corrosion resistance of the newly developed axle steels due to their finer microstructure and strongly adherent protective rusts.

According to the results of previous works (Ref 8), the corrosion resistance of pure iron and interstitial-free (or ultra-low carbon) steel has been reported to be very high because of the minor presence of carbides. On the other hand, in the case of medium and high carbon steels, the relative corrosion resistance has been reported to be low because the corrosion rate increases due to an increase in the cementite-to-ferrite area ratio (Ref 7, 10, 11). In this regard, Ferhat et al. (Ref 12) have reported that the corrosion rate of steel is strongly influenced by the amount of cementite and its morphological distribution on the ferrite phase. Katiyar et al. (Ref 13) have recently reported higher corrosion resistance for an air-cooled fully pearlitic steel due to its fine microstructure and reduction in interlamellar spacing leading to the uniform distribution of the galvanic couple. The corrosion resistance of a fully pearlitic steel can be further modified by altering the interlamellar spacing through the isothermal heat treatment process. However, the corrosion rates of the plain carbon steel having different microstructures

Prvan Kumar Katiyar and **K. Mondal**, Department of Materials Science and Engineering, Indian Institute of Technology, Kanpur 208 016, India; and **S. Misra**, Department of Civil Engineering, Indian Institute of Technology, Kanpur 208 016, India. Contact e-mail: kallol@iitk.ac.in.

(ferrite-pearlite, pearlite-martensite, spheroidized, tempered martensite and pearlite) have also been reported to be different due to different morphological features and distribution of the cementite (Ref 9, 14-16).

Katiyar et al. (Ref 17) have investigated the comparative corrosion behavior of five microstructures (pearlite, bainite, spheroidized, martensite and tempered martensite) made from a high carbon steel in freely aerated 3.5% NaCl solution. They have reported lower corrosion rate of the pearlitic steel and highest corrosion rate of the tempered martensite steel. However, the corrosion rate of bainite steel has been reported to be lower as compared to the spheroidized and the martensite steel. The variation in the corrosion rate of the steel having different microstructures has attributed to the size, shape and distribution of the ferrite and cementite phase (Ref 17).

Osório et al. (Ref 18) have observed lower corrosion rate of an IF steel than a low carbon steel. They have also reported substantial displacement of corrosion potential toward the nobler side in the IF steel, which is attributed to the absence of pearlite. Li et al. (Ref 19) have observed the microcell corrosion in a low carbon (0.15% C) ferrite-pearlite steel, and the corrosion rate has been compared with that of ferritic steels. They have reported higher corrosion tendency of the ferritic-pearlitic steel as compared to the ferritic steel due to the presence of pearlite, which acts as cathodes and ferrite phase becomes the anode and the ferritic-pearlitic steel suffers galvanic corrosion. However, in the case of the ferritic steels, similar grains reduce the probability of the formation of microcell corrosion (Ref 19). The morphologies of the different phases and % carbon would lead to change in the local electrochemical potential distribution, affecting the corrosion behavior of the steel (Ref 20). Choudhary et al. (Ref 21) have reported the effect of grain boundary on the corrosion behavior of a mild steel after rolling operation. The corrosion rate of the steel is mainly influenced by the presence of high-angle grain boundaries, whereas low-angle grain boundaries have limited effect on the corrosion behavior of the steel (Ref 21). There are other good numbers of studies on the effect of microstructures on the corrosion behavior of steel (Ref 18-25).

Though there are large number of studies on the effect of microstructures and compositions on the corrosion behavior of steel in the literature (Ref 9-25), it could be interesting to see the effect of carbon content from ultra-low (0.002%) to high (0.7%) carbon on the corrosion behavior of furnace cooled annealed carbon steels with nominal compositions in freely aerated 3.5% NaCl solution. Moreover, the effect of pearlite morphology within the pearlite colony on the corrosion behavior of carbon steel could also be an interesting addition to the existing knowledge in corrosion of steels.

Dynamic polarization, linear polarization and AC impedance spectroscopy tests have been used to find the relative corrosion rates of the steels. Hence, present work considers four carbon steels with carbon contents of 0.002, 0.17, 0.43 and 0.7% C in their annealed conditions to see the relative effect of carbon content and associated annealed microstructures on the dissolution behavior and corrosion mechanism. Annealed microstructure at different carbon level would be able to establish a relationship between the corrosion rate, fraction of pearlite (%), cementite-to-ferrite area ratio in pearlite and interlamellar spacing.

2. Experimental Procedure

2.1 Materials Preparation

2.1.1 Heat Treatments of the Selected Steel. The ultra-low carbon steel (IF steel) used for the current study was a cold-rolled annealed product and supplied by Tata Steels, India. The chemical composition of the ultra-low carbon (0.002% C), low carbon (0.17% C), medium carbon (0.43% C) and high carbon (0.7% C) steels used in the current study is listed in Table 1. The as-received IF steel was used for corrosion test without any further heat treatment. The samples of dimension 15 mm × 15 mm × 5 mm of the steels with carbon content from 0.17 to 0.7% C were cut and then homogenized at 950 °C in a muffle furnace for 12 min. After homogenization, the samples were allowed to cool in the furnace to obtain furnace annealed microstructures.

2.1.2 Hardness Tests and Microstructure of the Different Carbon Steels. In order to obtain the hardness and microstructures of the as-received IF steel and heat-treated steel samples, the samples were mechanically polished by silicon carbide papers up to 2500 grit size and followed by cloth polishing with 0.05 micron-sized alumina suspension. Prior to the microstructural observation, all the steel samples were etched by 3% Nital etchant solution. The micrographs of the etched steel samples were obtained by using field emission scanning electron microscopy (FE-SEM: Nova Nano SEM 450). FE-SEM of the corroded and un-etched samples was also carried out in the same instrument after the polarization tests. The Vicker's hardness measurements of the steel samples were performed using a Bareiss Prüfgerätebau GmbH hardness tester at a load of 100 g with the holding time of 10 s. Each reported hardness results are the average value of 10 different measurements at different locations of the steel sample.

### 2.2 Electrochemical Measurements of the Different Carbon Steel

The corrosion tests were performed in a conventional flat bottom cell using Parstat 2263 potentiostat (Princeton Applied Research, USA) with POWERCORR software. In polarization tests, a saturated calomel electrode (SCE) was used as a reference electrode, which had a constant potential of + 0.242 V with respect to the standard hydrogen electrode at room temperature. The counter electrode was a platinum mesh, while the mirror-polished steel specimen was used as working electrode. Before the polarization tests, the steel specimens were mechanically polished by silicon carbide papers up to 2500 grit size and followed by cloth polishing with alumina powder of size up to 0.05 microns suspended in water.

Figure 1 shows the schematic representation of the electrochemical cell setup. Polarization tests were performed in a freely aerated 3.5% NaCl solution at room temperature. The open-circuit potential (OCP) was measured for 2 h for stabilization, and the electrochemical impedance spectroscopy (EIS) test was carried out in a frequency range from 10^5 to 10^{-3} Hz with ± 10 mV of applied amplitude at corresponding OCP value. The impedance data were modeled with the help of Zsimpwin software (Princeton Applied Research, USA) and fitted with the appropriate equivalent circuit. The best fit of the EIS data was decided by the least chi-square (χ^2) value.

The linear polarization (R_p) tests were also carried out at electrode potential ranging ± 20 mV with respect to the OCP

Table 1 Compositions of the steels with different carbon contents (wt.%)

Materials	C	Si	Mn	P	S	Al	Ta	Ti	Fe
0.002% C	0.002	0.005	0.05	0.011	0.005	0.033	–	0.053	99.6
0.17% C	0.170	0.280	0.680	0.0210	0.021	0.034	–	–	98.7
0.43% C	0.436	0.188	0.758	0.0235	0.0413	0.0208	0.0739	–	98.3
0.70% C	0.708	0.239	1.12	0.0259	0.0208	0.0153	0.0725	–	97.7
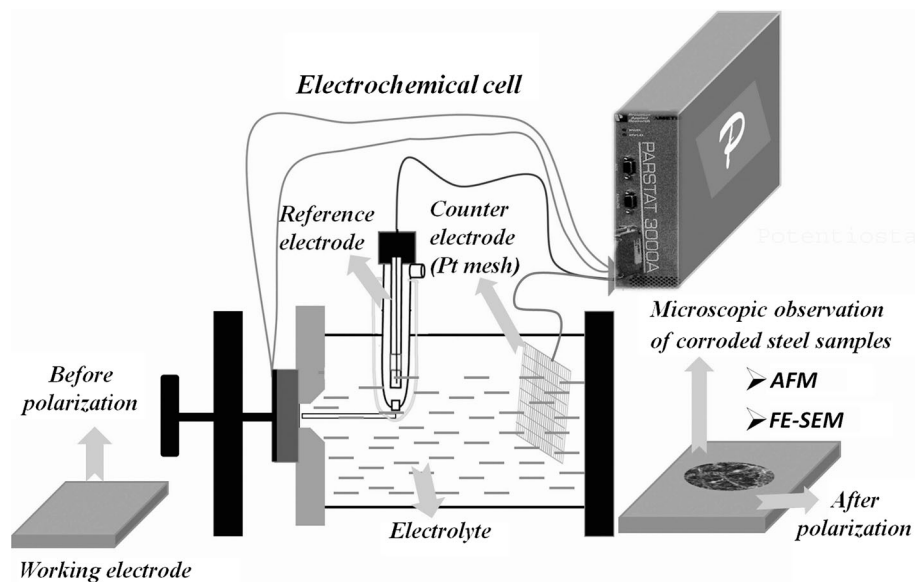
Fig. 1 Schematic representation of electrochemical cell setup

at the scan rate of 0.166 mV/s. For the measurement of polarization resistance (R_p), only the linear part of potential versus current density plot was used within the range of ± 10 mV (Ref 13). The slope of the over-voltage and current density at corrosion potential provided the value of linear polarization resistance by the following relation

$$R_p = \left(\frac{\Delta E}{\Delta i}\right)_{E=E_{corr}}$$

where ΔE was the change in the overpotential and Δi was the change in the current density.

The dynamic polarization tests were performed with a scan rate of 0.166 mV/s in the scan range from ± 250 mV, while all test results were reported with reference to the saturated calomel electrode (SCE) (ASTM G102) (Ref 26). The corrosion current densities of the different carbon steels were calculated from the polarization curve, and the corrosion rates of the steel samples were obtained by applying the following formula (Ref 27).

$$\text{Corrosion rate (mm/year)} = \frac{i_{corr} \times 0.00327 \times 27.92 \ (EW)}{7.86 \ (\rho)}$$

where i_{corr} was the corrosion current density in $\mu A/cm^2$, EW was the equivalent weight of Fe considering oxidation number to be 2 and ρ was the density of the selected steel (7.86 g/cm^3). All the experiments were repeated three times to ensure the reproducibility of the results.

2.3 Observation of Corroded Samples

FE-SEM and atomic force microscope (AFM) were used to understand the dissolution behavior and corrosion mechanisms of the plain carbon steels after polarization tests. Corroded samples obtained after polarization tests were rinsed with distilled water. Meanwhile, no corrosion products were observed on the polarized steel samples. Atomic force microscopy (AFM) was employed to examine the typical dissolution behavior of the corroded pearlitic (0.7% C) and ferrite-pearlite (0.17 and 0.43% C) steels after the polarization tests. The AFM was carried out in the contact mode with asylum research AFM (MFP3D) at a scan rate of 0.5 Hz.

3. Results and Discussion

3.1 Microstructural Observation of the Selected Steels

Ultra-low carbon or IF steel shows ferritic microstructure (Fig. 2a) with little presence of carbides in the matrix. The microstructures of typical ferrite-pearlite steels with carbon content of 0.17 and 0.43% are shown in Fig. 2(b) and (c), respectively. The fraction of pearlite varies according to the carbon content (Table 2) and has been calculated with the help of ImageJ software. Figure 2(d) shows the microstructure of fully pearlitic steel (0.7% C). The average thickness of the cementite plate, interlamellar spacing and colony size of the
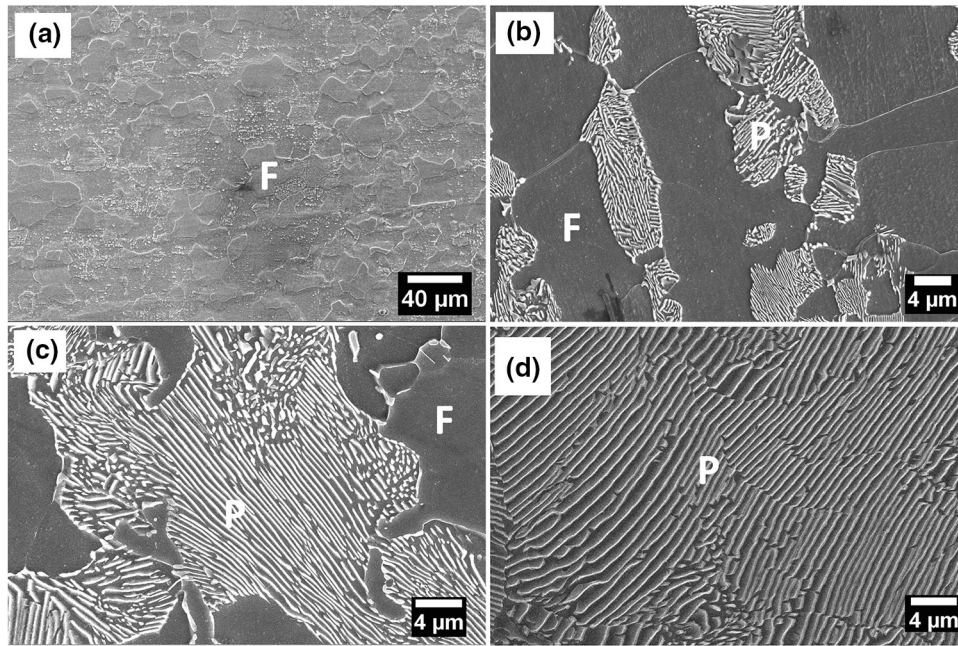
Fig. 2 FE-SEM micrographs of the annealed steels with different carbon contents showing ferrite (F) and cementite phase in gray and white color, respectively: (a) 0.002% C (IF steel), (b) 0.17% C (mild steel with ferrite/pearlite microstructure), (c) 0.43% C (medium carbon, ferrite/pearlite steel) and (d) 0.70% C (high carbon pearlitic (P) steel). Etchant is 3% Nital

Table 2 Properties of the annealed steels with carbon contents

| Material | Phases of steel | | | | | | |
	Fraction of Pearlite	Fraction of ferrite	Cementite thickness, nm	Ferrite thickness, nm	Interlamellar spacing, nm	Cementite/Ferrite area ratio, Pearlite	Hardness, Vickers
0.17% C low carbon steel	~ 32.74%	~ 67.26%	184.2 ± 46.80	547.1 ± 71.38	731.3 ± 74.7	0.336	217 ± 6
0.43% C medium carbon steel	~ 52.34%	~ 47.66%	126.7 ± 14.66	246.60 ± 52.25	373.3 ± 61.42	0.514	251 ± 9
0.7% C high carbon steel	~ 100% Pearlite	~	106.45 ± 32.89	177.03 ± 49.72	283.48 ± 61.17	0.601	339 ± 6

pearlite has also been calculated with the help of ImageJ software (Table 2). Vickers hardness values of the steel samples corresponding to four steels with 0.002, 0.17, 0.43 and 0.7% C have been measured to be 110 ± 5, 217 ± 6, 251 ± 9 and 339 ± 6 HV, respectively. The average pearlite colony size of the 0.17% C steel is 26.62 µm, which is larger than that of the medium carbon steel (18.38 µm), while the average pearlite colony size of fully pearlitic steel has been measured to be 34.34 µm under identical processing condition. The average values of the interlamellar spacing of the pearlite have been measured to be 731.3 ± 74.7, 373.3 ± 61.42 and 283.48 ± 61.17 nm in the steels with 0.17, 0.43 and 0.7% carbon, respectively. The values of the cementite-to-ferrite area ratio in the pearlite have been measured to be 0.336, 0.514 and 0.601 for the steels with 0.17, 0.43 and 0.7% C, respectively.

3.2 Electrochemical Results of Different Carbon Steels

3.2.1 Polarization Curves. Figure 3 shows the dynamic polarization curves for the steel samples with different carbon contents (0.002, 0.17, 0.43 and 0.7% C) tested in freely aerated 3.5% NaCl solution. Various polarization parameters, such as open-circuit potential (OCP), corrosion potential (E_{corr}), cathodic slope (β_c), corrosion current density (i_{corr}) and corrosion rate (mm/y), are presented in Table 3. Figure 3 shows that the cathodic slope (β_c) of the polarization curves increases with the carbon contents. It is also clear that the polarization is concentration polarization controlled and this indicates that the corrosion rate is a function of limiting oxygen cathodic current density for all the steels. Since it is freely aerated neutral NaCl solution, limiting oxygen cathodic current density is quite plausible, where the cathodic reaction is

$O_2 + H_2O + 4e = 4OH^-$. The anodic or dissolution reaction $(Fe = Fe^{+2} + 2e^-)$ takes place preferentially at the ferrite regions since ferrite is anodic as compared to the cathodic cementite (Fe_3C) zone. It can be observed that the corrosion rate increases with the carbon content (Table 3). The IF steel has got the lowest corrosion rate or the highest corrosion resistance among all the steels. However, an increase in the corrosion rate is sluggish with the carbon content for the steel samples of 0.17, 0.43 and 0.7% C. On the other hand, the corrosion potential (E_{corr}) of the IF steel in Table 3 shows almost similar E_{corr} as observed by Singh et al. (Ref 1). The E_{corr} decreases in the steel with 0.17% C due to the introduction of pearlite in the steel. Thereafter, the E_{corr} increases with the increase in carbon content (0.43% and 0.7% C steels) and subsequent increase in the pearlite content. Similar behavior has been noticed for the OCP (Table 3).

Osório et al. (Ref 19) have also observed similar and significant change in corrosion potential for an IF steel (-629 mV) and for a low carbon steel (-705 mV). The corrosion potential shifts toward the nobler side in case of the IF steel due to the absence of pearlite (%). They have also attributed this behavior to the presence of pearlite (27%) in the low carbon steel. Distribution of pearlitic colony throughout the ferritic matrix provides a number of sites of pearlite and ferrite inducing galvanic corrosion (Ref 19). The pearlite content or in other words, cementite content also increases with the increase
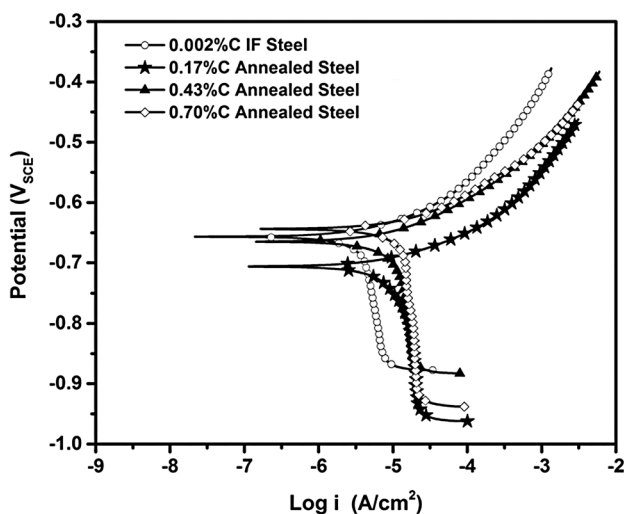

Fig. 3 Polarization plots for the annealed steels with different carbon contents (0.002, 0.17, 0.43 and 0.7% C) in freely aerated 3.5% NaCl solution at a scan rate of 0.166 mV/s

in carbon content from 0.002 to 0.7% C steel (Fig. 2a-d). Interestingly, the cathodic slopes of the polarization plots as shown in Fig. 2(a) and Table 3 increase gradually from -655 to -1661 mV/decade of current density with the increase in carbon content from 0.002 to 0.7% C, respectively. Therefore, it is very much evident that the increase in the cathodic slope is due to the cementite in the steels with the increase in carbon content. Therefore, the catalytic activity of cementite on enhancing the oxygen reduction reaction is due to the increase in % pearlite, and it also leads to an increase in the corrosion rate in low alloy plain carbon steel.

3.2.2 Electrochemical Impedance Spectroscopy (EIS) Measurements. The impedance spectra of all the steel samples are shown in Fig. 4. An equivalent circuit consisting of R_s $(Q_{EDL}$ $R_c)$ (Fig. 4d) shows good fit for different carbon steels having least chi-square (χ^2) value in the range of 9.2×10^{-4} to 1.13×10^{-3} confirming the best fit of the $(R_s(Q_{EDL}R_c))$ circuit. Evolution of base microstructures without etching just after polarization (shown later) also indicates that rust formation is minimal during polarization. Therefore, it is logical to have only one time constant in the form of capacitance of the electrical double layer. Here, Q_{EDL} refers to the constant phase elements (CPE) and C is double-layer capacitance, R_s solution resistance and R_c charge transfer resistance at the metal/electrolyte interface (Ref 14, 28, 29).

The EIS parameters obtained by an equivalent circuit fitting are listed in Table 4. The fitting results reveal that the R_c values of the different carbon steel decrease when carbon content increases. The charge transfer resistance (polarization resistance) values are obtained from the diameter of the Nyquist plots (Fig. 4a) and also from the frequency-independent horizontal section of the Bode magnitude plots (Fig. 4b). The Nyquist plots show the single time constant and it is also confirmed by Bode phase plots.

The Nyquist plot of the 0.002% C steel has got the highest charge transfer resistance among all the other steel samples, and it corroborates well with the lowest corrosion rate of the 0.002% C steel as measured from polarization results (indicated in Fig. 3 and Table 3). Similarly, the charge transfer resistance decreases gradually in case of the steels with carbon content of 0.17, 0.43 and 0.7%. A decrease in the value of the charge transfer resistance (R_c) could be a sign of the continued dissolution of the active ferrite phase. The Bode magnitude, as well as phase plots, is shown in Fig. 4(b) and (c), respectively. The high-frequency region of the bode magnitude plots provides information about the electrolyte resistance, and low-frequency region gives information about the charge transfer resistance. The charge transfer resistance of the 0.002% C steel is 4096 Ω cm^2 and decreases in the following

Table 3 Values of OCP, cathodic slope, i_{corr}, E_{corr} and corrosion rates as obtained from electrochemical polarization in freely aerated 3.5% NaCl solution

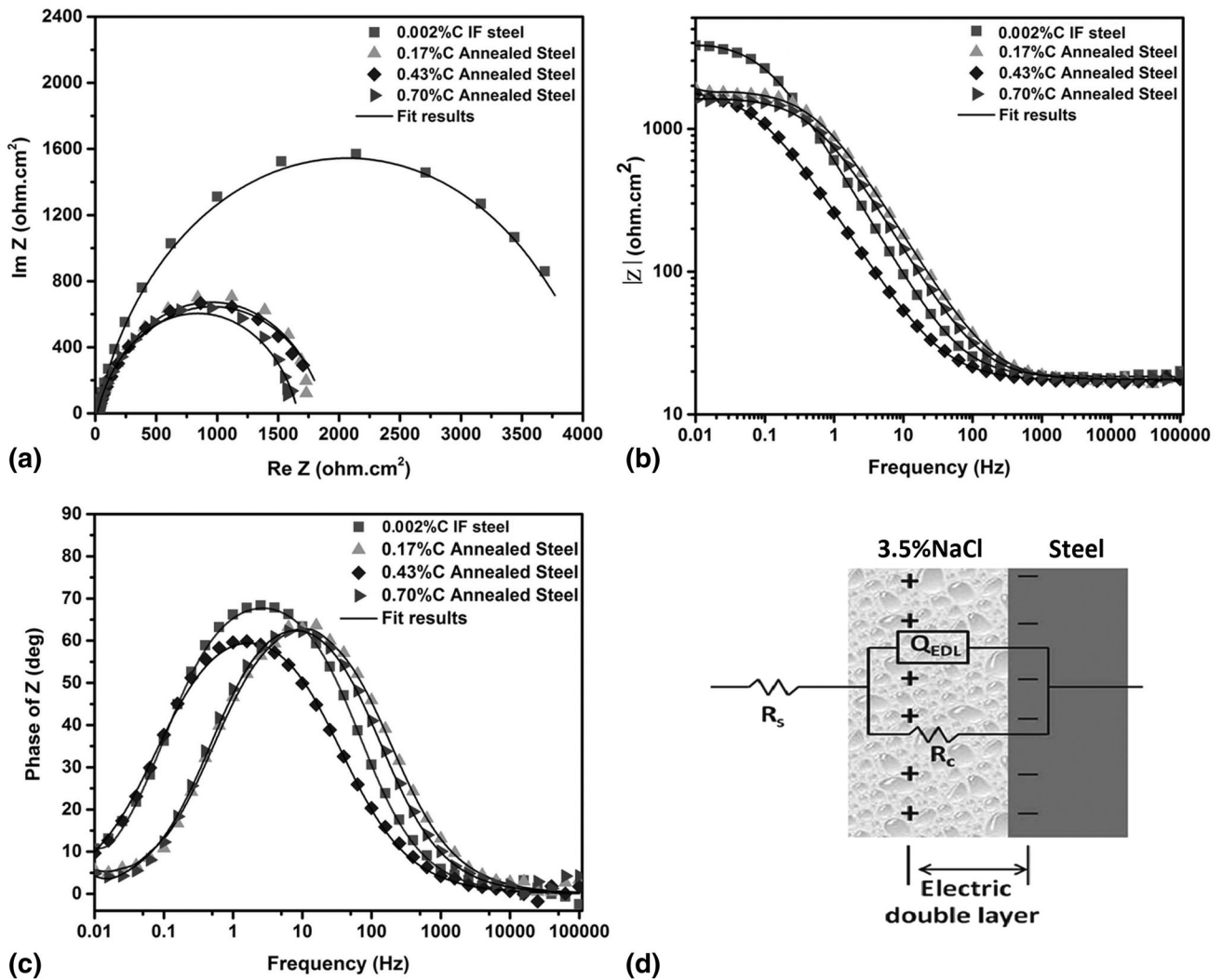| Materials	OCP, mV$_{SCE}$	Cathodic slope, mV$_{SCE}$/decade	i_{corr}, μA/cm^2	E_{corr}, mV$_{SCE}$	Corrosion rate, mm/y
0.002% C Ultra-low carbon	-626	-655.3	3.77	-644.2	0.044 ± 0.01
0.17% C Low carbon steel	-715	-854.1	11.88	-700.4	0.137 ± 0.05
0.43% C Medium carbon steel	-635	-1156.3	12.81	-664.1	0.15 ± 0.01
0.7% C High carbon steel	-690	-1661.2	14.55	-643.2	0.17 ± 0.02

Fig. 4 (a) Nyquist plots, (b) Bode magnitude plots, (c) Bode phase plots and (d) electrical equivalent circuit model used for fitting EIS data for the annealed steels with different carbon contents (0.002, 0.17, 0.43 and 0.7% C) in free aerated 3.5% NaCl solution

Table 4 Different electrical parameters obtained after equivalent circuit fitting to the EIS data obtained at OCP in freely aerated 3.5% NaCl solution (Percent error is mentioned in the parentheses.)

Materials	R_s, Ω cm^2	Q, Ω^{-1} s^n cm$^{-2} \times 10^{-4}$	n	R_c, Ω cm^2	X^2, Chi squared
0.002% C	18.37	3.47	0.83	4096	9.2×10^{-4}
Ultra-low carbon	(0.79)	(1.38)	(0.44)	(1.68)	
0.17% C	17.15	1.95	0.80	1892	1.62×10^{-3}
Low carbon steel	(1.16)	(2.64)	(0.68)	(1.51)	
0.43% C	17.25	8.99	0.77	1870	4.6×10^{-3}
Medium carbon steel	(0.69)	(1.25)	(0.48)	(1.52)	
0.7% C	17.58	2.38	0.81	1647	1.13×10^{-3}
High carbon steel	(0.94)	(2.16)	(0.58)	(1.29)	

sequence: 0.17% C (1892 Ω cm^2)—0.43% C (1870 Ω cm^2)—0.7% C (1647 Ω cm^2). The mid-frequency region of the bode magnitude plots is dominated by the capacitance, which is high in the case of 0.002% C steel as compared to other steels. It is also confirmed by the Bode phase plot for the IF steel, and this is associated with higher phase angle (closer to

68.54°) and a higher capacitive response has been noticed for the IF steel as compared to other steels (see in Fig. 4c). The maxima for 0.17, 0.43 and 0.7% C steels are 63.40, 60.17 and 61.86, respectively. All are pointing that the steel with the lowest carbon content has higher corrosion resistance, and other steels have comparable corrosion resistance.
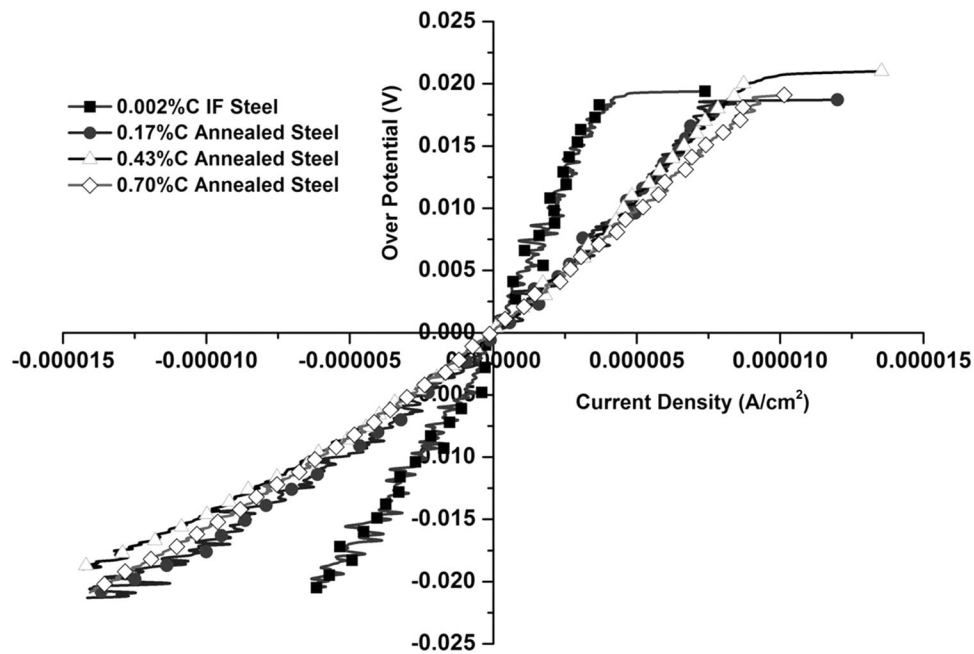
Fig. 5 Linear polarization plots of the annealed steels with different carbon contents (0.002, 0.17, 0.43 and 0.7% C)
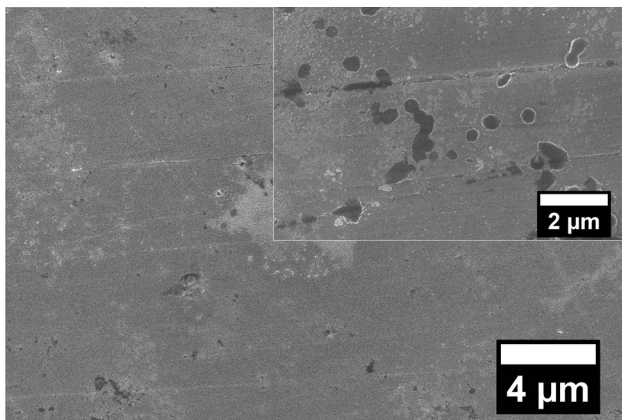

Fig. 6 FE-SEM micrographs of 0.002% C (IF steel) after polarization test in freely aerated 3.5%NaCl solution. The inset shows the magnified image. The microstructures are result of polarization and no etching has been used after polarization

Fig. 7 FE-SEM micrographs of the annealed steel with 0.17% C after polarization test in freely aerated 3.5%NaCl solution. The inset shows the magnified image. The microstructures are result of polarization and no etching has been used after polarization

3.2.3 Linear Polarization Resistance (R_p) Measurements. Figure 5 shows the linear polarization plots of all the four carbon steels. Polarization resistance (R_p) values obtained from Fig. 5 follow the same trend as that of the R_c obtained from EIS (Table 4). The value of R_p for 0.002% C steel (4737 Ω cm^2) has been found to be very high as compared to other steels and decreases in the following sequence: 0.17% C (2110 Ω cm^2)—0.43% C (2010 Ω cm^2)—0.7% C (1834 Ω cm^2). Moreover, the R_p values of the steels are observed to be inversely proportional to their corrosion rates (Fig. 3 and Table 3).

3.3 Corrosion Morphology

Figure 6 shows the morphology of the surface of the IF steel after polarization test. It shows uniform corrosion with the presence of scatt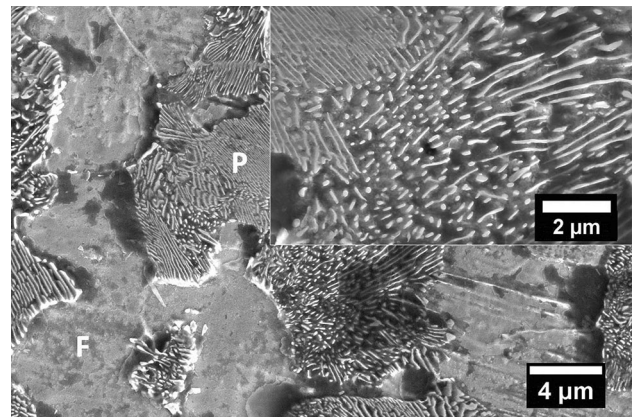ered localized attacked regions (inset). Since the IF steel is predominantly ferritic with local presence of very fine alloy carbides, the carbides can lead to local galvanic cells initiating local corrosion susceptible region. Figure 7 shows the anodic dissolution behavior of the low carbon steel (0.17% C). The ferritic lamellae as well as polygonal ferrite dissolve due to their anodic nature. However, the dissolution of ferrite lamellae is more pronounced since it is with galvanic coupling with the cementite lamellae, which act as cathodic component, where cathodic reaction happens (Ref 30-32). The inset of Fig. 7 shows the difference in dissolution behavior. Moreover, the pearlitic colonies have a pop up nature on the surface as compared to the polygonal ferrite grains since pearlitic region contains cementite lamellae, which are richer in carbon. This morphological difference between ferrite and pearlitic zone is very much evident near the encapsulated ferrite in pearlite (P region in Fig. 7).
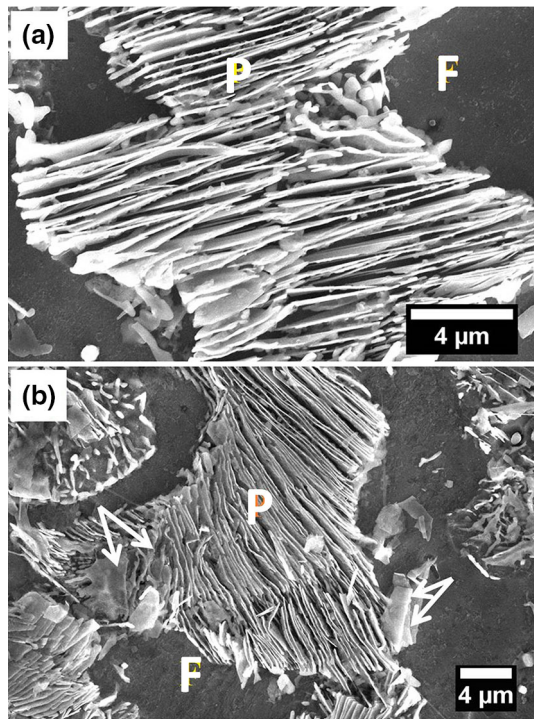
Fig. 8 FE-SEM micrographs of the annealed steel with 0.43% C after polarization test in freely aerated 3.5%NaCl solution. The microstructures are result of polarization and no etching has been used after polarization
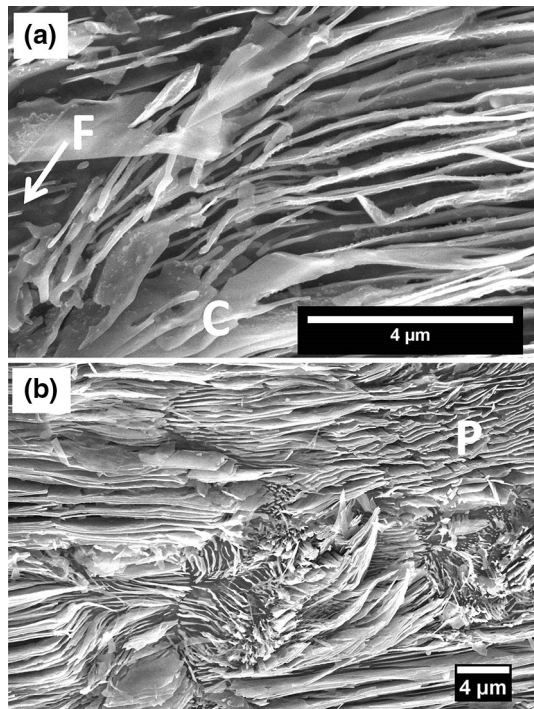

Fig. 9 FE-SEM micrographs of the annealed steel with 0.7% C after polarization test in freely aerated 3.5% NaCl solution. The microstructures are result of polarization and no etching has been used after polarization

Similar trend in dissolution pattern has been observed in case of the steel sample with carbon content 0.43% (Fig. 8a and

b). However, the only difference is in the degree of attack in the polygonal ferritic region as well in the ferrite lamellae in pearlite. Since the area fraction of the ferrite is less (0.43% C steel), the pop up of the pearlitic zone is more pronounced. In addition to that, some cementite lamellae have separated from the pearlite colony as shown by an arrowhead in Fig. 8(b).

Figure 9(a) and (b) shows the intensive anodic dissolution of the ferrite lamellae and associated skeleton of the cementite phase in the fully pearlitic steel (0.7% C). Since the pearlite content is ∼ 100% in 0.7% C steel, the size of the cementite plates could impart a significant effect on the corrosion rate. Even the interfacial area between cementite and ferrite lamellae could also decide the corrosion rates (Ref 8, 13). The corrosion rate of the 0.7% C steel is the highest among all the steels in the present study. Hence, it can be stated that the higher cementite-to-ferrite interfacial area ratio and the presence of 100% pearlite could be attributed to the highest corrosion rate in the 0.7% C steel. However, the increase in the corrosion rate of the steels with an increase in carbon content from 0.17 to 0.7% C is not significantly different. It is clear that the lowest carbon containing IF steel has very low corrosion rate, which is mainly attributed to the presence of only ferrite. Similar results have been also reported by Al-Hassan et al. (Ref 31). They have found pure iron is less susceptible to corrosion as compared to a low alloy plain carbon steel and the corrosion rate increases with an increase in carbon content. They have also observed that the microstructure and the chemical composition of the steel play a dominant role in order to determine the corrosion behavior of steel (Ref 31). However, in the present work, the nominal composition of all the four steels as well as similarly heat-treated microstructures actually indicate the effect of carbon content and annealed microstructures on corrosion only.

Therefore, the corrosion rate of the steels with the presence of pearlite, partially or fully, must have counter-influencing behavior mainly due to the difference in three factors: pearlite fraction, interlamellar spacing between the ferrite and the cementite phase and cementite-to-ferrite interfacial area ratio in pearlite.

Figure 10(a)-(f) shows the AFM images of the corrosion surface of the steels with carbon 0.17 to 0.7% after polarization without any etching. Figure 10(a) and (b) show the dissolution pattern in the steel with 0.17% C. In Fig. 10(a), it can be clearly noticed that the pearlitic colonies are protruded as compared to the ferrite grains (shown by arrowheads). Figure 10(b) shows the relative dissolution of the ferrite and cementite lamellae in a pearlite colony. It is also evident that the ferrite lamellae have corroded more as compared to the cementite lamellae.

Figure 10(c) shows corrosion attack pattern in the steel with 0.43% C. Here also ferrite grains are attacked more as compared to the pearlite colonies (Fig. 10d). Similarly, the ferrite lamellae corrode more as compared to the cementite lamellae. This is natural since pearlite acts as cathodic when galvanically connected to ferrite grain and in the pearlite colony, the cementite lamellae are cathodic part as compared to the ferrite lamellae. Interestingly, the cementite lamellae try to separate out due to excessive corrosion at the base of the lamellae and align on the corroded surface as it can be observed in Fig. 10(d).

Finally, Fig. 10(e) and (f) shows the corrosion attack pattern on the pearlitic colonies in the steel with 0.7% C. Ferrite lamellae dissolve more. No ferrite grains can be noticed since it is fully pearlitic steel. It is very clear from Fig. 10(f) that many
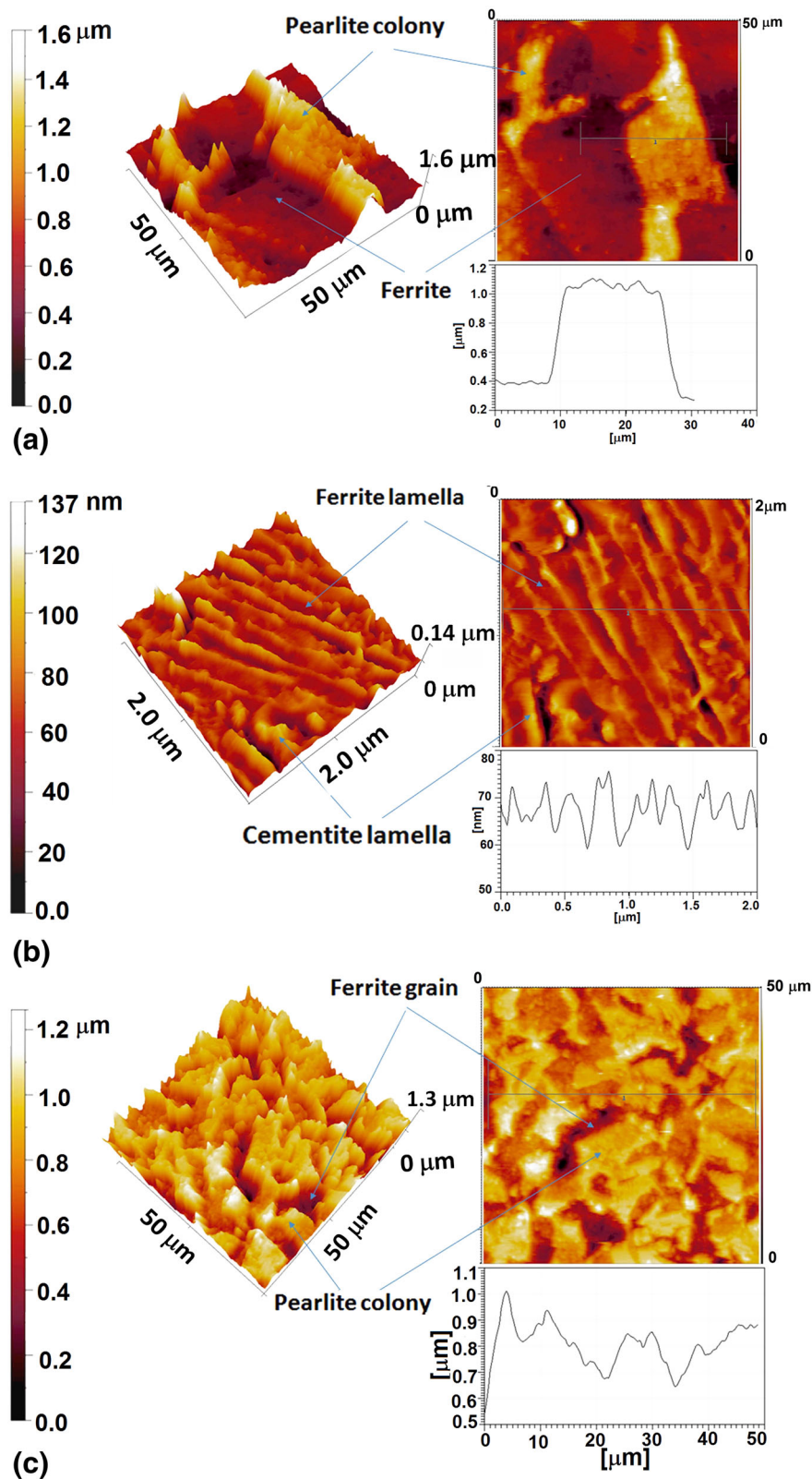
Fig. 10 AFM images of the corroded surfaces in the carbon steels in NaCl solution. Figures (a) and (b) show the ferrite grain and pearlite colony as well as ferrite and cementite lamellae, respectively, in the 0.17% C steel. Figures (c) and (d) show the ferrite grain and pearlite colony as well as ferrite and cementite lamellae, respectively, in the 0.43% C steel and Figures (e) and (f) show the dissolution behavior of the pearlitic colony in fully pearlitic steel. The microstructures are the result of polarization and no etching has been used after polarization
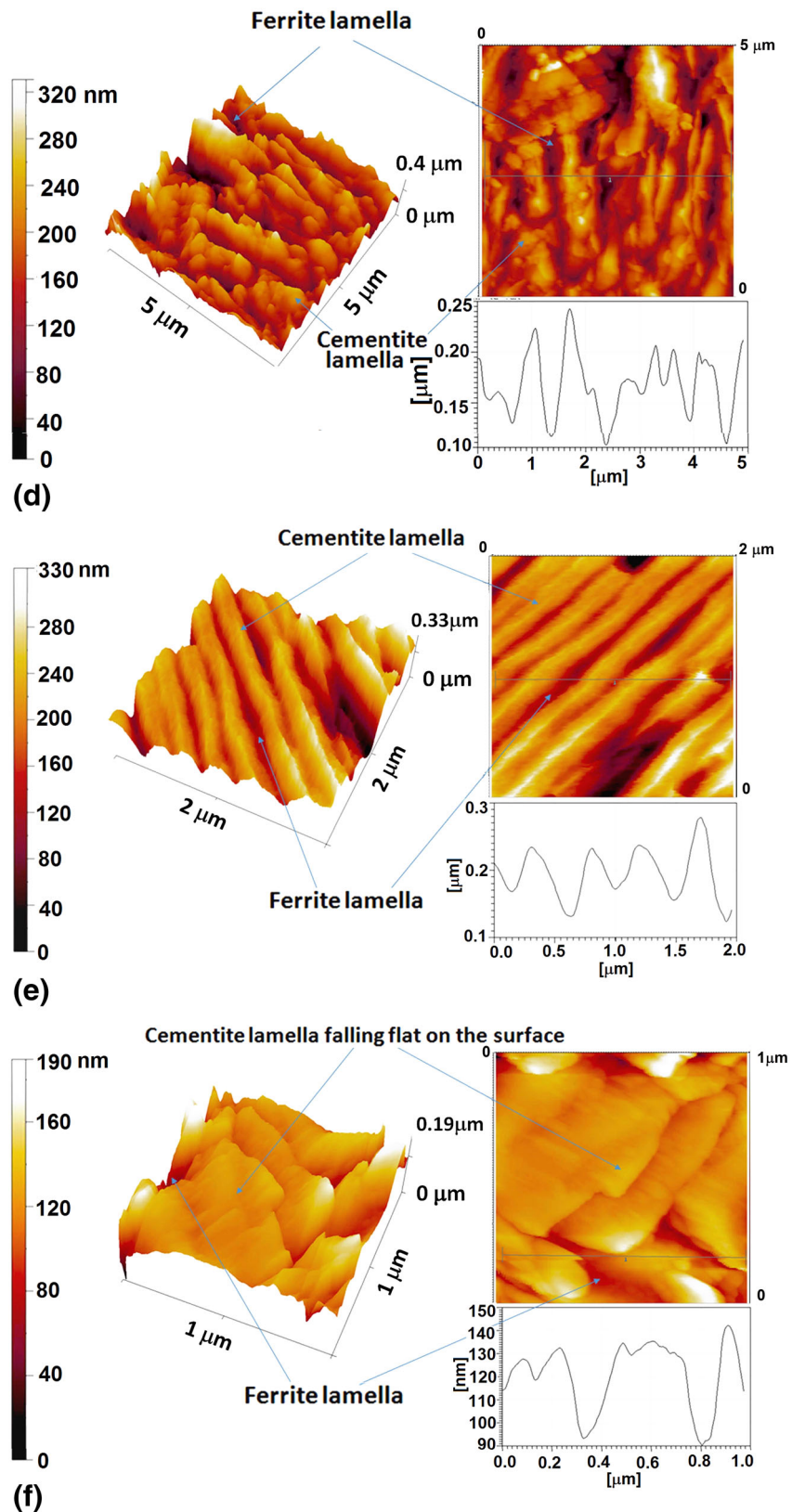
Fig. 10 continued

of the cementite plates are covering up the surface. This is also visible in Fig. 9. The cementite plates align on the surface because of finer interlamellar spacing in the 0.7% C steel. Moreover, as compared to the 0.43% C steel, the 0.7% C steel has finer interlamellar spacing. Hence, the coverage of the surface with aligned cementite plates on the corroded surface is more in the later steel. Once the surface is covered with cementite plates, which is the manifestation of finer interlamel-

lar spacing, the further corrosion needs to be occurring through the fine capillary formed between the side-by aligned cementite plates. Hence, corrosion would get sluggish.

It is worth mentioning that the FE-SEM micrographs (Fig. 6-9) as well as AFM images (Fig. 10) are obtained after dynamic polarization in 3.5% NaCl solution and without etching. This is possible due to the active dissolution as observed in the polarization plots in Fig. 3. Moreover, absence of passivation on the surface of the steels in 3.5% NaCl solution allows the surface to be clean from any oxide layer and morphologies of the microstructures in four steels could be visible after polarization test and that too without etching. One more interesting thing could be observed from FE-SEM micrographs (Fig. 7-9) that the severity of dissolution of ferrite lamellae decreases with the decrease in the interlamellar spacing. Since pearlite content and subsequently cementite content (Table 2) increases rapidly with the increase in carbon content, initially, the side-by ferrite lamellae would experience rapid dissolution. However, once the dissolution of ferrite lamellae starts, the surface is covered by the cementite plates making it predominantly cathodically covered and further corrosion is hindered. Coverage of the surface with cementite plates has been clearly shown in Fig. 10(d) and (f). This is very clear from the progression of the cementite covering on the surface of the 0.17 to 0.7% C steels (Fig. 7-9). This should also increase the corrosion potential or OCP, and interestingly, the corrosion potential also increases with the change in carbon from 0.17 to 0.7% (Table 3). This would definitely try to reduce overall corrosion rate. Hence, it can be stated that the increase in total pearlite fraction as well as cementite-to-ferrite area ratio would increase the corrosion rate, whereas finer interlamellar spacing would decrease the corrosion rate. It has been shown earlier by the same authors (Ref 13) that the finer pearlitic structure imparts better corrosion resistance. Hence, the severity of dissolution of the interlamellar ferrite decreases with the decrease in interlamellar spacing.

It is interesting to notice that the R_p values of the annealed steels with different carbon contents (0.002, 0.17, 0.43 and 0.7% C) depend on the carbon (%), cementite-to-ferrite area ratio in the pearlitic region and fraction of pearlite. The values of polarization resistance (R_p) obtained from linear polarization of four carbon steels (Fig. 5) and impedance spectroscopy (R_c) (Fig. 4a) have been found to decrease significantly from the ultra-low carbon steel (0.002%) to low carbon steel (0.17%) due to an increase in % pearlite content (Table 2). However, the decrease in polarization resistance is insignificant with the increase in carbon content from the low carbon (0.17% C) to the medium (0.43% C) and the high carbon (0.7% C) steels (Fig. 4a and 5). It could be attributed to the fact that the increase in the fraction of pearlite and cementite-to-ferrite area ratio in pearlite tries to decrease the polarization resistance. However, the decrease in interlamellar spacing tries to increase the polarization resistance.

Similarly, the increase in polarization resistance up to certain fineness in pearlite has also been observed by Katiyar et al. (Ref 13), where the effect of cooling rate on the corrosion behavior of pearlitic steels with varying interlamellar spacing in the pearlite region in aerated 3.5% NaCl solution has been discussed. Because of this counteracting effect, the resultant polarization resistance decreases slowly with the increase in carbon (%). It could be a reason for negligible difference in corrosion rates in the steels with the presence of pearlite with reference to the variation in fraction and morphology of pearlite
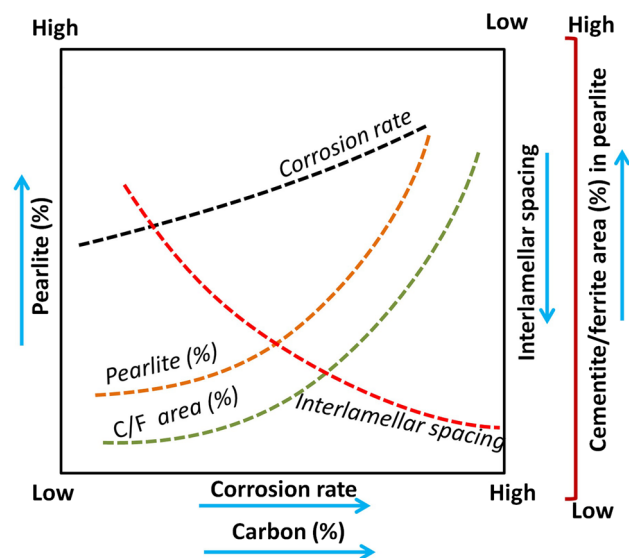

Fig. 11 Schematic representation of corrosion behavior of the annealed steels with different carbon contents (0.002, 0.17, 0.43 and 0.7% C) showing the relationship between the corrosion rate with carbon (%), fraction of pearlite (%), cementite/ferrite area ratio and interlamellar spacing

as observed in the present work. Osório et al. (Ref 18) could also observe that the fine pearlite lamellae with lower interlamellar spacing are comparatively less susceptible to corrosion as compared to the coarser pearlite (Ref 18).

Figure 11 shows the schematic representation of the corrosion behavior of all the steels with different carbon contents (0.002, 0.17, 0.43 and 0.7% C) and relationship between the corrosion rate with carbon (%), fraction of pearlite (%), cementite-to-ferrite area ratio and interlamellar spacing. The corrosion rate of the steels with the presence of pearlite has been observed to be a balance between the fraction of pearlite (%), interlamellar spacing and cementite-to-ferrite area ratio in pearlite.

The corrosion rate obtained from four carbon steels has been found to increase greatly from the ultra-low carbon steel (0.002%) to the low carbon steel (0.17%) due to the appearance of pearlite. Increase in the pearlite content and cementite-to-ferrite area ratio in pearlite enhances the corrosion rate, while interlamellar spacing, which decreases with the increase in carbon content in the steels, tries to reduce the corrosion rate (Ref 13). Therefore, the overall corrosion rate increases slowly with an increase of carbon (%) (shown in Fig. 11). Hence, the corrosion behavior of the annealed steels with different carbon contents (0.002, 0.17, 0.43 and 0.7% C) has been found to be counter-influencing nature depending on the distribution, fineness and fraction of the pearlite.

4. Conclusions

In the present study, it can be concluded that the corrosion rate of the plain carbon steel mainly depends upon the % carbon, fraction of the pearlite (%), cementite-to-ferrite area ratio in pearlite and interlamellar spacing. The corrosion rates of the steel with different carbon contents follow the sequence

in increasing order: ultra-low carbon steel (0.002% C)—low carbon steel (0.17% C)—medium carbon steel (0.43% C)—high carbon steel (0.7% C). This follows the exact opposite trend of the charge transfer resistance (R_c) of the samples obtained from EIS measurements and the polarization resistance (R_p) obtained from linear polarization. The corrosion rate of the steel increases greatly from the IF steel to the steel with 0.17% C because of the introduction of pearlite in the later. However, the increase in corrosion rate is marginal with the increase in carbon content from the low carbon to the medium and the high carbon steels because of counteracting influence from the fraction of pearlite, cementite-to-ferrite area ratio and interlamellar spacing. Increase in the fraction of pearlite and cementite-to-ferrite interfacial area ratio in pearlite tries to increase the corrosion rate. However, the decrease in inter-lamellar spacing tries to decrease the corrosion rate. Hence, the overall corrosion rate increases slowly with an increase of carbon (%). The microstructural observation after polarization in four annealed steels without the aid of etching could effectively enable to understand the corrosion mechanism in carbon steels with varying carbon content.

References

1. G.P. Singh, A.P. Moon, S. Sengupta, G. Deo, S. Sangal, and K. Mondal, Corrosion Behavior of IF Steel in Various Media and Its Comparison with Mild Steel, *J. Mater. Eng. Perform.*, 2015, **24**, p 1961–1974
2. H.L. Cai, J.S. Mou, and Z.Y. Hou, Microstructure, Texture and Property of Interstitial-Free (IF) Steel After Ultra-Fast Annealing, *Adv. Mater. Res.*, 2015, **1120–1121**, p 1003–1007
3. P.K.S. Babu, A. Mathiazhagan, C.G. Nandakumar, Corrosion Health Monitoring System for Steel Ship Structures, *Int. J. Environ. Sci. Dev.*, 2014, **5**, p 491–495
4. B.L. Bramfitt, *Structure/Property Relationships in Irons and Steels*, ASM International, Metals Handbook Desk Edition, Second Edition., 1998, pp. 153–173
5. G.S. Frankel, *Corrosion: Fundamentals, testing, and protection*, ASM Handbook, Geauga, 2003
6. V.M. Kardonskii, G.V. Kurdyumov, and M.D. Perkas, Effect of the Size and Shape of Cementite Particles on the Structure and Properties of Deformed Steel, *Met. Sci. Heat Treat.*, 1964, **6**, p 62–68
7. F. Sun, X. Li, and X. Cheng, Effects of Carbon Content and Microstructure on Corrosion Property of New Developed Steels in Acidic Salt Solutions, *Acta Metall. Sin. (Engl. Lett.)*, 2014, **27**, p 115–123
8. H.J. Cleary and N.D. Greene, Corrosion Properties of Iron and Steel, *Corros. Sci.*, 1967, **7**, p 821–831
9. A.P. Moon, S. Sangal, S. Srivastav, N.S. Gajbhiye, and K. Mondal, Passivation and Corrosion Behavior of Modified Ferritic-Pearlitic Railway Axle Steels, *J. Mater. Eng. Perform.*, 2015, **24**, p 85–97
10. S.N. Saltykov and N.V. Tarasova, Anodic Dissolution of Ferrite Phases from Iron-Carbon Ferrite-Cementite Alloys with Different Forms of Cementite, *Prot. Met.*, 2006, **42**, p 542–547
11. D.N. Staicopolus, The Role of Cementite in the Acidic Corrosion of Steel, *J. Electrochem. Soc.*, 1963, **110**, p 1121
12. M. Ferhat, A. Benchettara, S.E. Amara, and D. Najjar, Corrosion Behaviour of Fe-C Alloys in a Sulfuric Medium, *J. Mater. Environ. Sci.*, 2014, **5**, p 1059–1068
13. P.K. Katiyar, S. Misra, and K. Mondal, Effect of Different Cooling Rates on the Corrosion Behavior of High-Carbon Pearlitic Steel, *J. Mater. Eng. Perform.*, 2018, **4**, p 1753–1762
14. A.P. Moon, S. Sangal, S. Layek, S. Giribaskar, and K. Mondal, Corrosion Behavior of High-Strength Bainitic Rail Steels, *Metall. Mater. Trans. A Phys. Metall. Mater. Sci.*, 2015, **46**, p 1500–1518
15. S.N. Saltykov and M.S. Putilina, The Effects of the Cementite Phase of Iron-Carbon Alloys on Their Electrochemical Behavior in an Oxalic Acid Medium, *Prot. Met.*, 2006, **42**, p 406–411
16. D. Clover, B. Kinsella, B. Pejcic, and R. De Marco, The Influence of Microstructure on the Corrosion Rate of Various Carbon Steels, *J. Appl. Electrochem.*, 2005, **35**, p 139–149
17. P.K. Katiyar, S. Misra, and K. Mondal, Comparative Corrosion Behavior of Five Microstructures (Pearlite, Bainite, Spheroidized, Martensite, and Tempered Martensite) Made from a High Carbon Steel, *Metall. Mat. Trans. A*, 2019, **50**, p 1489–1501
18. W.R. Osório, L.C. Peixoto, A. Garcia, Electrochemical corrosion behaviour of a Ti-IF steel and a SAE 1020 steel in a 0.5M NaCl solution, *Mater. Corros.*, 2010, **61**, p 407–411
19. J. Li, H. Su, F. Chai, D. Xue, L. Li, X. Li, and H. Meng, Corrosion Behavior of Low-Carbon Cr Micro-Alloyed Steel for Grounding Grids in Simulated Acidic Soil, *J. Iron. Steel Res. Int.*, 2018, **25**, p 755–766
20. A. Moon, S. Sangal, and K. Mondal, Corrosion Behaviour of New Railway Axle Steels, *Trans. Indian Inst. Met.*, 2013, **66**, p 33–41
21. S. Choudhary, V. Nanda, S. Shekhar, A. Garg, and K. Mondal, Effect of Microstructural Anisotropy on the Electrochemical Behavior of Rolled Mild Steel, *J. Mater. Eng. Perform.*, 2017, **26**, p 185–194
22. K.D. Ralston and N. Birbilis, Effect of Grain Size on Corrosion: A Review, *Corrosion*, 2010, **66**, p 75005–75013
23. A.R. Tourky, A.A.A. Azim, and M.M. Anwar, Effect of Carbon Content on the Corrosion and Passivity of Iron, *Corros. Sci.*, 1965, **5**, p 301–317
24. R. Balasubramaniam, B. Panda, G. Dwivedi, A.P. Moon, S. Mahapatra, A.K. Manuwal et al., Alloy Development of Corrosion-Resistant Rail Steel, *Curr. Sci.*, 2011, **100**, p 52–57
25. B. Panda, R. Balasubramaniam, G. Dwivedi, and S. Mahapatra, Corrosion of Novel Rail Steels in 3.5% NaCl Solution, *Trans. Indian Inst. Met.*, 2008, **61**, p 177–181
26. ASTM, Standard Test Method for Conducting Potentiodynamic Polarization Resistance Measurements, ASTM G59-97, 2014, p 1–4
27. ASTM, Standard Practice for Calculation of Corrosion Rates and Related Information, ASTM G-102, 1999, **89**, p 1–7
28. A. Lasia, *Electrochemical Impedance Spectroscopy and Its Applications*, Springer, New York, 2014
29. V.F. Lvovich, *Impedance Spectroscopy: Applications to Electrochemical and Dielectric Phenomena*, Wiley, New York, NY, 2012
30. W.R. Osório, L.C. Peixoto, L.R. Garcia, and A. Garcia, Electrochemical Corrosion Response of a Low Carbon Heat Treated Steel in a NaCl Solution, *Mater. Corros.*, 2009, **60**, p 804–812
31. S. Al-Hassan, B. Mishra, D.L. Olson, and M.M. Salama, Effect of Microstructure on Corrosion of Steels in Aqueous Solution Containing Carbon Dioxide, *Corros. Eng. Sect.*, 1998, **54**, p 480–491
32. R. Cabrera-Sieraa, N. Batina, and I. Gonzalez, Electrochemical Characterization of Pearlite Phase Oxidation of 1018 Carbon Steel in a Borate Medium Using ECSTM Technique, *J. Electrochem. Soc.*, 2005, **152**, p 534–539